arXiv:1402.1927v1 [cond-mat.supr-con] 9 Feb 2014

Modeling the nanoscale linear response of superconducting thin films measured by a scanning probe microwave microscope

Tamin Tai[1,2], B. G. Ghamsari[2], and Steven M. Anlage[1,2]
[1] *Department of Electrical and Computer Engineering, University of Maryland, College Park, Maryland 20742-3285, USA and*
[2] *Department of Physics, Center for Nanophysics and Advanced Materials, University of Maryland, College Park, Maryland 20742-4111, USA*

(Dated: February 11, 2014)

A localized and strong RF magnetic field, created by a magnetic write head, is used to examine the linear electrodynamic properties of a Nb superconducting film. The complex reflection coefficient of the write head held in close proximity to the films is measured as a function of sample temperature. A model combining a magnetic circuit (magnetic write head inductively coupled to the sample) and transmission line (microwave circuit) is given to interpret the linear response measurement. Additionally, this reflection linear response measurement can be used to determine the temperature dependence of the magnetic penetration depth on a variety of superconductors.

PACS numbers:

I. INTRODUCTION

Investigation of superconducting properties such as magnetic penetration depth (λ), critical temperature (T_c) and critical field (H_c) is very important because it yields valuable information about superconducting materials for a variety of applications. Generally, the critical temperature and critical field of a superconductor can be measured straightforwardly by performing a standard current-voltage (I-V) and magnetization-field (M-H) measurement, respectively. For the magnetic penetration depth λ of a superconductor, various experimental methods have been developed and are summarized in Ref [1] in detail. For example, in order to get an accurate estimation of the absolute value of λ, Josephson tunneling junctions can be fabricated for a measurement of the Fraunhofer diffraction pattern [2][3][4]. The main disadvantage of this method is the requirement of fabrication of tunnel junctions for each material of interest. Another precision method is to measure the resonant frequency of a superconducting resonator structure such as the end-plate resonator [5], parallel plate resonator [1] or dielectric resonator [6][7][8] and then calculate the change in absolute λ. One limitation of this method is that it requires a model for the temperature dependence of the penetration depth, or an independent determination of the absolute value of λ at some temperature. For both of these methods, the absolute λ is assumed to be a global value common to the entire sample. This assumption is often faulty, especially for newly-developed materials with inhomogeneous properties, or for well-established materials containing defects. We seek to go beyond these simple characterization techniques and develop a spatially-resolved measurement of electrodynamic properties.

Our objective is to examine thin films for use in future superconducting radio frequency (SRF) accelerator cavities, and to understand which defects limit their performance at high RF fields. A reflection method combined with scanning probe technology is used to determine the local λ of superconducting materials and to study the homogeneity of the electrodynamic properties. For example, the technology of magnetic force microscopy has been used to study the local λ in the pnictide and unconventional superconductors recently [9]. Additionally, scanning SQUID susceptometry has been applied to precisely measure the change of local λ for novel unconventional superconductors [10][11]. However none of the techniques described above can be applied to SRF materials at high RF field and in the GHz regime [12]. The field generated by SQUID susceptometry is not strong enough and spatial resolution degrades at frequencies in the GHz range [13], limiting its application in high field and high frequency study. It is of interest to study SRF materials under conditions of strong RF field excitation, approaching the critical field. Our objective here is to examine the homogeneity of the fundamental electromagnetic properties of candidate SRF materials such as T_c and λ under localized excitation at the operating conditions of SRF cavities to understand the drop of quality factor (Q) of SRF cavities in the medium-field and high-field regimes [12][14]. The promising candidate materials for SRF cavities are Nb films and MgB_2 films [15][16] in addition to bulk Nb [12].

Based on this motivation, we developed a novel scanning probe microscope by combining a magnetic writer and a near field-microwave microscope [17][18]. The magnetic writer can create a localized and strong RF magnetic field on the surface of the superconducting samples and should achieve surface fields $B_{surface} \sim 10^2\ mT$ and sub-micron resolution at a frequency of several GHz [19][20]. The design concept is similar in spirit to previous studies of magnetic write heads used to measure ferromagnetic materials [21][22][23]. What we measure is a reflection signal from the localized area of the superconductor by performing an S_{11} measurement, which is the ratio of the reflected voltage to the incident voltage, with a vector network analyzer (VNA). Due to the tempera-

ture (T) dependent magnetic penetration depth $\lambda(T)$ and surface resistance of the measured materials, the reflected voltage will also change with temperature. Although a similar measurement was done on the high T_c cuprates by loop probes with a loop diameter on the millimeter scale [24], our measurement uses a magnetic write head on the sub-micron scale which will generate more intense and localized magnetic fields on the surface of the superconductor. Therefore, many field-dependent parameters, such as the surface reactance, can be measured by applying different RF magnetic fields at different temperatures up to a scale on the order of the thermodynamic critical field H_c. The change of S_{11} under different RF magnetic fields and temperatures allows one to calculate the change in surface reactance as a function of the RF field and temperature. In this way, the temperature and RF field-dependent penetration depth λ also can be obtained.

II. EXPERIMENT

A. Linear Response Setup

The schematic setup for the linear response measurements is shown in Fig.1. A microwave fundamental tone (V_{a1}^{+}) at a given frequency is sent from port 1 of the vector network analyzer (VNA) (model ♯ Agilent N5242A) into the magnetic writer (from Seagate PINNACLE heads manufactured in 2010 for perpendicular recording technology). The linearly reflected signal (at the same frequency), V_{b1}^{-}, in port 1 of the VNA is measured and the complex reflection coefficient $S_{11} = V_{b1}^{-}/V_{a1}^{+}$ is determined.

The process is now discussed in more detail. The magnetic writer is used as a scanning probe which is integrated into our microwave circuit by soldering the probe assembly on to a coaxial cable. For this probe, the main part of the writer is a magnetic yoke surrounded by a several-turn helical coil which transforms the incident signal into magnetic flux. The yoke is made of a high permeability material (usually ferrite) to channel the magnetic flux to the narrow gap. It is also shielded to define a nano-scale bit in the recording medium during the writing process [25][26][27]. A close-up schematic view of the magnetic write head probe on a superconducting sample is shown on the side of Fig. 1. In our design, the magnetic writer approaches the surface of the superconductor in the range of 200 $nm \sim 2$ μm. The fundamental tone stimulates the magnetic writer to generate an RF magnetic field and therefore excites a screening current on the sample surface so that it can maintain the Meissner state in the bulk of the material. Larger magnetic field induces stronger screening current within the penetration depth (λ) of the superconducting surface, until the field reaches the critical field of the material. The time dependent screening current on the superconductor will induce an electromotive force (emf) back on the magnetic writer at the same frequency as the excitation. (Note that we do not measure a signal from the magnetic reader element of the write head because it is too far away from the localized excitation on the surface of the superconductor.) The emf will couple with the incident fundamental tone and reflect back as an output signal (V_{b1}^{-}). We measure the ratio of V_{b1}^{-} to V_{a1}^{+} (S_{11}) at different temperatures of the superconducting samples. The sample temperature is controlled by a Lakeshore 340 temperature controller.

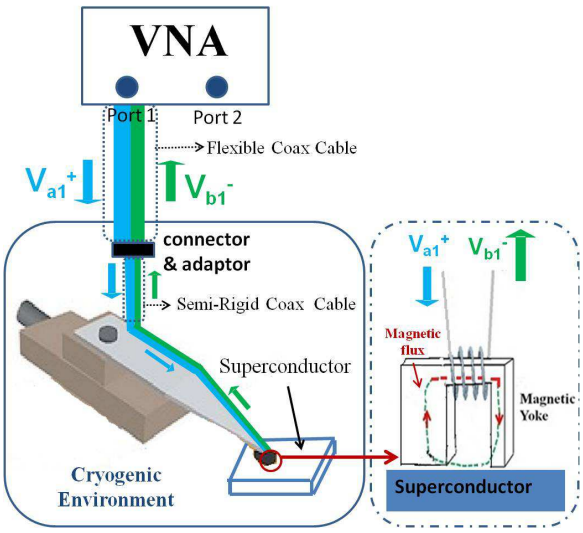

FIG. 1: Schematic diagram of the linear response measurement, S_{11}, performed as a function of sample temperature with the vector network analyzer (VNA). The reflected signal (V_{b1}^{-}) and incident signal (V_{a1}^{+}) are at the same frequency. The inset shows a schematic model of the magnetic write head.

Many single-position measurements on different superconducting samples were performed. Before cooling down to measure the superconducting reflection signal, an electronic calibration (Ecal) is performed at the end of the flexible coaxial cable at ambient temperature and ambient pressure (black line labeled "connector & adapter" in Fig. 1). A part of semi-rigid coax cable on the probe assembly cannot be calibrated with Ecal in the measurement. After drawing a vacuum, the cooling procedure is followed and it takes several hours to stabilize temperature down to almost 4.2 K (without pumping on the helium exhaust), and then the measurement is performed.

B. superconducting samples

The superconducting samples we study are Nb thin films with thickness 50 nm. Nb films are made by sputtering Nb onto 3 inch diameter quartz wafers at ambient temperature under $1.5 * 10^{-3}$ torr argon pressure. After the deposition, the wafer is diced into many 10*10 mm^2 pieces but otherwise left un-disturbed. The T_c of each piece is 8.3 K, which is measured by performing a standard DC resistance measurement. The tested sample is well anchored to the cold plate to ensure that the

surface temperature of the Nb superconductor is close to that of the cold plate. The probe is held by a three axis translatable arm. Hence different points on the surface of the sample can be examined in the same cool-down. We tested multiple locations on 3 Nb films, and all pieces show consistent results for their linear response measurement.

III. LINEAR RESPONSE MEASUREMENT

A. Frequency Response of the Magnetic Probe Assembly

In the high frequency regime, impedance matching of the magnetic probe to the system impedance is a key issue to maximize signal level at the sample. Many different probes were tested and show different suitable operating frequency regimes to satisfy the matching condition for the microwave microscope system [28]. Additionally, different probes will have different resonant frequencies after integrating the probe to the microwave system. The resonant frequency of the probe is also a height dependent parameter due to the variable degree of coupling between the sample and the probe at different separations. Fig. 2 shows the frequency dependent S_{11} measurement of the PINNACLE probe under -15 dBm (considered low power) excitation and at a single-position on one of the Nb films. The measurements are taken at two different temperatures: one is in the Nb normal state (10 K) and the other is in the Nb superconducting state (below the T_c of the film). The probe-sample separation, which can be approximately judged by the resonant frequency of the probe assembly, is estimated to be on the order of $0.2 \sim 1\ \mu m$ from our previous measurements and modeling on many superconducting thin films [18][19]. First, one can clearly see that the deepest dip in $|S_{11}|$ vs frequency happens around 2 GHz, at which the maximum rf magnetic field at the sample can be generated. Second, the $|S_{11}|$ amplitude of the deepest dip is very sensitive to the superconducting transition temperature of the Nb films. From the inset of Fig. 2, one can see a significant change of S_{11} amplitude ($\left|\Delta\,|S_{11}|\right|$) around the dip frequency when the sample becomes superconducting. This measurement can determine the best excitation frequency and the maximum sensitivity at a specific height while the probe approaches the superconducting sample.

B. Temperature Dependence of S_{11} on Nb Thin Film

The dot-circle points in Fig. 3 (a) and Fig. 3 (b) shows the amplitude and phase of a temperature dependent S_{11} measurement, respectively, at a single-position on one of the Nb films under -15 dBm, 1.98 GHz excitation by the PINNACLE probe. Note that the excitation frequency

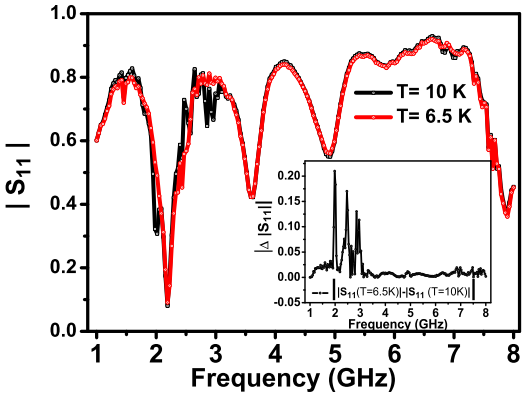

FIG. 2: Frequency dependence of $|S_{11}|$ in linear scale measured at two different temperatures by the PINNACLE probe. The sample under test is a Nb thin film with thickness 50 nm and T_c=8.3 K. The excitation power in both measurements is -15 dBm. The inset shows the absolute value of difference between $|S_{11}|$ at 6.5 K and $|S_{11}|$ at 10 K.

in the measurement is decided by the resonant dip in the frequency dependent S_{11} measurement as shown in Fig. 2. One can see a sharp change of S_{11} that occurs around normalized temperature $T/T_c = 1$ for both the amplitude and phase. This change indicates the Nb transition temperature (T_c). Physically, at this temperature, the Nb thin film becomes superconducting and generates a strong screening current on the sample surface which couples with the incident voltage (V_{a1}^{+}) and results in a change of the reflected voltage (V_{b1}^{-}). In other words, from the normal state to the superconducting state, the surface reactance suddenly changes at the superconducting critical temperature. The solid curve in Fig.3 (a) and Fig. 3 (b) are the outcome of complex S_{11} curve fitting for amplitude and phase respectively based on the model that will be provided below to quantitatively interpret the temperature dependent S_{11} measurement.

IV. MODELING THE LINEAR RESPONSE MEASUREMENT

For modeling this $S_{11}(T)$ measurement, a Meissner state in the superconductor is assumed while the temperature is below T_c. The magnetic yoke is excited by a current in the N-turn solenoid to channel a magnetic flux, Φ, down to the gap as illustrated in Fig. 4 (a). The separation between the probe and the sample is assumed to be small compared to the magnetic gap length (l_g), and is ignored in the model. While exciting the surface of a superconductor by the magnetic probe, there are two channels for flux in the magnetic circuit: the air gap and the penetration depth of the superconductor. Since the total flux, Φ, provided by the yoke of the magnetic write-head distributes among these two channels, they should

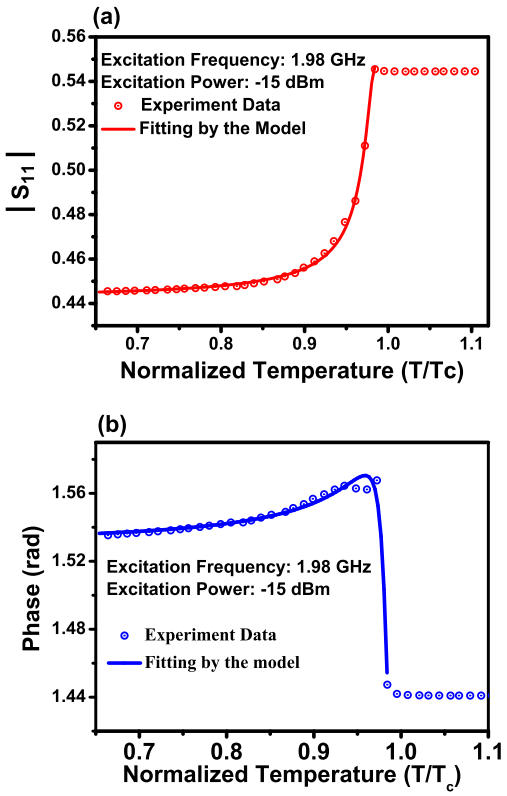

FIG. 3: (a)Experimental amplitude of temperature dependent S_{11} of a 50 nm Nb thin film is plotted in dot circle symbols measured with the PINNACLE probe at 1.98 GHz, -15 dBm excitation. Note $|S_{11}|$ is plotted on a linear scale. The solid line indicates the theoretical amplitude of S_{11} based on the model described in the text. (b) Dot circle symbols are the corresponding temperature dependent phase of the experimental S_{11}. The solid line indicates the theoretical phase of S_{11} based on the model. Both theoretical curves in (a) and (b) are plotted with αl=0.245 (unit-less), Z_1=30.23 Ω, R_{Bkd}=320.48 Ω, X_{Bkd}=-105.13 Ω, N/R_g=6.59 $*$ 10^{-9} $Henry$ and μ_0/μ_f= -0.46 under constant values nl=0.065 m, d_{yoke}=500 nm and T_c=8.3 K.

be represented by two parallel reluctances, R_g and R_s, as shown in Fig. 4 (b). The gap reluctance, R_g, follows the conventional geometrical definition of reluctance

$$R_g = \frac{l_g}{\mu_0 A_{gap}} = \frac{l_g}{\mu_0 l_y d_{yoke}} \qquad H^{-1} \tag{1}$$

where A_{gap} is the effective cross-sectional area of stray flux in the air gap, d_{yoke} is the effective thickness of the stray flux channel inside the air gap (Note that d_{yoke} is analogous to the thickness of the magnetic yoke in the ring shape head for longitudinal recording), l_y is the the size of the yoke in the transverse dimensions (see Fig. 4). The Meissner state reluctance R_s is generated due to the penetration of magnetic field into the superconductor within its Meissner screening region. Therefore, the total flux will shunt into two branches, Φ_s with its reluctance R_s and Φ_g with its reluctance R_g. In the linear Meissner

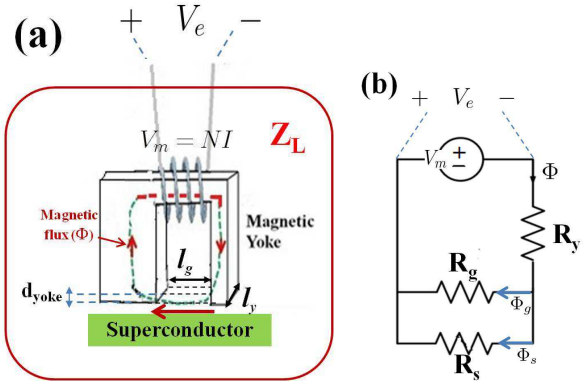

FIG. 4: (a) A schematic of the experiment where a magnetic probe locally excites the surface of a superconductor with a time-varying magnetic field. The probe can be modeled as an electrical load impedance, Z_L. This figure uses the ring shaped magnetic yoke to schematically represent the writer. l_g indicates the length of the gap under the bottom of the magnetic yoke. d_{yoke} is the effective thickness of the stray magnetic flux in the air gap and l_y is the size of the yoke in the transverse dimensions. V_m is the impressed voltage created by the N turn solenoid with input current I. V_e is the induced electric voltage on the input winding. (b) The equivalent **magnetic circuit** of the experiment with a superconducting sample and the magnetic probe. Φ_g is the magnetic flux going through the gap reluctance R_g and Φ_s is the magnetic flux going through the superconducting sample with reluctance R_s in the Meissner state. Φ is the total flux in the magnetic circuit. V_m and V_e have the same description as in Fig. 4 (a).

state, we obtain

$$\begin{aligned} \Phi_g &= B * A_{gap} = B * (l_y * d_{yoke}) \\ \Phi_s &= B * (l_y * \lambda(T)) \end{aligned} \tag{2}$$

where B is the amplitude of the applied RF magnetic field in the gap (assumed to be the same field witnessed by the sample) and $\lambda(T)$ is the temperature dependent penetration depth. By applying the node-voltage law, we have Φ_g R_g = Φ_s R_s. Hence, the reluctance of the linear Meissner state is given by

$$R_s = \frac{d_{yoke}}{\lambda(T)} R_g \qquad where \;\; R_g = \frac{l_g}{\mu_0 l_y d_{yoke}} \tag{3}$$

So the total reluctance in this magnetic circuit is

$$\begin{aligned} R_{eq} = R_y + R_g // R_s &= R_y + \frac{d_{yoke}}{d_{yoke} + \lambda} R_g \\ &= \left(\frac{\mu_0}{\mu_f} + \frac{d_{yoke}}{d_{yoke} + \lambda} \right) R_g \end{aligned} \tag{4}$$

where R_y is the reluctance of the magnetic yoke and can be approximated as $\frac{\mu_0}{\mu_f} R_g$, here μ_0 and μ_f indicate the permeability of the vacuum and the magnetic yoke, respectively. By solving the magnetic circuit in Fig. 4, one

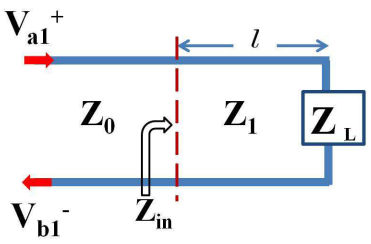

FIG. 5: Model the electrical impedance looking into a magnetic write head probe at the end of a short segment of transmission line. Z_0 indicates the characteristic impedance of the calibrated transmission line (50 Ω). Z_1 is the characteristic impedance of the probe transmission line (usually not 50 Ω) with length l. Z_L represents the load impedance including the impedance of the magnetic probe head and a superconducting sample. V_{a1}^{+} and V_{b1}^{-} indicate the input and reflected microwave tones respectively.

finds the magnetic flux flowing through the magnetic circuit will, in turn, give the induced electric voltage into the input winding through Faraday's law

$$V_e = \frac{d\Phi}{dt} = \frac{d}{dt}\left(\frac{V_m}{R_{eq}}\right) = \frac{d}{dt}(\frac{NI}{R_{eq}}) = \frac{iN\omega I_0 e^{i\omega t}/R_g}{\mu_0/\mu_f + d_{yoke}/(d_{yoke}+\lambda(T))} \tag{5}$$

where V_m is the impressed voltage on the magnetic circuit and can be written as $V_m = NI$. Here N is the number of turns in the solenoid and I indicates the RF input current with a maximum amplitude I_0 in an RF cycle ($I = I_0 e^{i\omega t}$). Therefore the impedance of the magnetic circuit can be found as $\frac{iN\omega/R_g}{\mu_0/\mu_f + d_{yoke}/(d_{yoke}+\lambda(T))}$. To evaluate the microwave load impedance presented by the write head, Z_L , one should include the impedance coming from the rest of the probe circuit to get

$$Z_L = Z_{Bkd} + \frac{i\omega N/R_g}{\frac{\mu_0}{\mu_f} + \frac{d_{yoke}}{d_{yoke}+\lambda(T)}} \; ; \; Z_{Bkd} \equiv R_{Bkd} + iX_{Bkd} \tag{6}$$

where R_{Bkd} and X_{Bkd} represent the background resistance and reactance of the load impedance, respectively (i.e. these parameters model the background probe-dependent properties of the write head). Note that the load impedance model does not include the loss in the superconductor. In addition, while the film thickness is smaller than the penetration depth, the regular penetration depth should be replaced by an effective penetration depth, λ_e [2]

$$\lambda(T) \to \lambda_e(T) = \frac{\lambda^2(T)}{d_{film}} \tag{7}$$

where d_{film} is the thickness of the film and it is assumed that $d_{film} \ll \lambda$.

In the experiment schematically shown in Fig. 1, the probe load impedance (represented now by Z_L) is connected to a printed circuit board and then a semi-rigid coax cable of finite length is soldered to the contacts of the printed circuit board. The length of the printed circuit board plus the length of semi-rigid coax cable can be combined together and treated as a transmission line of length l on the probe assembly. One can model the microwave circuit of a transmission line terminated by Z_L as shown in Fig. 5. In this one port measurement, the microwave calibration is done only on the transmission line from the part of the flexible coax cable shown in Fig. 1 but not on the probe assembly. A characteristic impedance mismatch between the calibrated transmission line and the un-calibrated part will be inevitable. Here Z_0 represents the characteristic impedance of the calibrated transmission line, 50 Ohms in our case, and Z_1 is the characteristic impedance of the un-calibrated transmission line on the probe assembly with a length of l. Both Z_0 and Z_1 are real. In this circumstance, the input impedance, Z_{in} is the impedance seen at the plane of calibration, given by,

$$Z_{in} = Z_1 \frac{Z_L + jZ_1 tan(\gamma l)}{Z_1 + jZ_L tan(\gamma l)} \;\; where \;\; \gamma = \beta - i\alpha = \frac{n\omega}{c} - i\alpha \tag{8}$$

Here n is the refractive index of the transmission line of length l, ω is the angular frequency and α is an attenuation coefficient inside the transmission line. Finally the theoretical S_{11} based on this model can be calculated as

$$S_{11} = \frac{Z_{in} - Z_0}{Z_{in} + Z_0}, \tag{9}$$

and compared to experiment.

Complex curve fitting of this model to the $S_{11}(T)$ data is performed by the least square method to minimize the difference between the experimental temperature dependent S_{11} values and the values predicted by the model. The details of the complex curve fitting method for the linear response measurement are discussed in Ref. [28].

For the curve fitting, the index of refraction of the Teflon inside the coaxial cable in our experiment is taken to be $n \approx 1.2$, independent of the excitation frequency. The un-calibrated length of the transmission line is around 5∼6 cm. Conveniently, we combine the n and l together to treat them as a constant term $nl = 0.065$ m in the calculation. On the other hand, the coefficient α (unit: m^{-1}) and l (unit: m) are bundled together as a dimensionless fitting parameter. The effective thickness of stray field in the air gap is assumed to be a constant, d_{yoke}=500 nm. The temperature dependence of an effective penetration depth, λ_e, is approximately described by [2]

$$\lambda_e(T) \approx \frac{\left(\lambda(0)\left[1-(T/T_c)^4\right]^{-\frac{1}{2}}\right)^2}{d_{film}} \tag{10}$$

where $\lambda(0) = 40\ nm$ is the 0 K penetration depth of Nb and $d_{film} = 50\ nm$ is the known thickness of the measured Nb thin film. The transition temperature T_c=8.3 K

is kept fixed for the fit. Therefore, based on the model, the unknown coefficients in the experiment are αl, Z_1, R_{Bkd}, X_{Bkd}, N/R_g and μ_0/μ_f.

The fit is done on the data set measured by the PINNACLE probe on the 50 nm Nb film with an excitation frequency of 1.98 GHz as discussed above. The solid lines in Fig. 3 (a) and Fig.3 (b) show the theoretical amplitude and phase respectively, based on the model with the following fit coefficients : $\alpha l = 0.245$ (unit-less), $Z_1 = 30.23\ \Omega$, $R_{Bkd} = 320.48\ \Omega$, $X_{Bkd} = -105.13\ \Omega$, $N/R_g = 6.59 * 10^{-9}\ Henry$ and $\mu_0/\mu_f = -0.46$. Again, the experimental data for the amplitude and phase is indicated in the figure by dot circles and the fit is excellent. Note that the μ_0/μ_f is a negative value, which implies that the excitation frequency is above and not far away from the yoke ferrite ferromagnetic resonance frequency. All of the fitting coefficients are physically reasonable. The sensitivity of the fits to variation of the fixed parameters in the fitting was also studied. For example, the variation of d_{yoke} from 200 nm to 1 μm will make a change in the μ_0/μ_f, R_{Bkd}, and X_{Bkd} values with $\pm 15\%$ variation. The N/R_g parameter varies by $\pm 1\%$ and is on the order of 10^{-9} $Henry$, not very sensitive to the change of d_{yoke} and the rest of the fixed parameters. Finally, note that the model is designed only to fit the data in the superconducting state. In the normal state, the penetration depth $\lambda(T)$ in Eq. 6 should change to the skin depth of the normal state of Nb. In this case, the field configuration around the sample is very different, and the situation is of not of interest to us here.

V. DISCUSSION

With this model, the magnitude and temperature dependence of the magnetic penetration depth of any superconducting thin film can be calculated after all of the parameters in the fit are calibrated by a standard thin film. Then a raster scan on the surface of superconductor at constant height will successfully image the contrast of λ of any superconducting thin film. The lateral length scales measured with this probe are on the order of the gap length l_g, or probe-sample separation, whichever is greater [18][19]. However compared with a nonlinearity measurement, the linear response measurement is not as sensitive to the extrinsic electromagnetic response associated with defects on superconductors [19][20][29]. Another limitation for the linear response measurement is the fact that we could not develop signals from bulk Nb surfaces. The reason is that the surface reactance in thin films is more significant than that of bulk superconductors, as illustrated in Eq. 7, which leads to a measurable change in the linear response of Nb thin films but not on bulk Nb. This limitation further motivates the need to pursue localized nonlinear measurements to get information about bulk superconductors [17][18][19][20].

VI. CONCLUSIONS

From the linear response measurement of Nb thin films by a magnetic write head probe, the electrodynamic properties of Nb can be identified. The linear response can also be used to find the film T_c in a local area. A magnetic circuit model combined with the transmission line circuit is given to interpret the linear response measurement. From the curve fitting results, many unknown coefficients in our microwave circuit can be fixed. This model will enable quantitatively imaging of the microwave surface properties of superconducting materials.

VII. ACKNOWLEDGEMENTS

This work is supported by the US Department of Energy / High Energy Physics through grant # DESC0004950, and also by the ONR AppEl, Task D10, (Award No. N000140911190), and CNAM.

[1] V. V. Talanov, L. V. Mercaldo, S. M. Anlage, and J. H. Claassen, Review of Scientific Instruments **71**, 2136 (2000).
[2] M. Tinkham, *Introduction to Superconductivity* (McGraw-Hill, New York, 2004), 2nd ed.
[3] A. Barone and G. Paternò, *Physics and Applications of Josephson Effect* (Wiley, 1982).
[4] D. Cunnane, C. Zhuang, K. Chen, X. X. Xi, J. Yong, and T. R. Lemberger, Appl. Phys. Lett. **102**, 072603 (2013).
[5] N. Klein, G. Muller, H. Piel, B. Roas, L. Shultz, U. Klein, and M. Peininger, Appl. Phys. Lett. **54**, 757 (1989).
[6] N. Klein, J. Supercond. **5**, 195 (1992).
[7] C. Wilker, Z.-Y. Shen, V.-X. Nguen, and M. S. Brenner, IEEE Trans. Appl. Supercond. **3**, 2832 (1992).
[8] Y. Kobayashi and H. Yoshikawa, Microwave Theory Tech. **46**, 2524 (1998).
[9] L. Luan, O. M. Auslaender, T. M. Lippman, C. W. Hicks, B. Kalisky, J.-H. Chu, J. G. Analytis, I. R. Fisher, J. R. Kirtley, and K. A. Moler, Phys. Rev. B **81**, 100501 (2010).
[10] C. W. Hicks, T. M. Lippman, M. E. Huber, J. G. Analytis, J.-H. Chu, A. S. Erickson, I. R. Fisher, and K. A. Moler, Phys. Rev. Lett. **103**, 127003 (2009).
[11] J. R. Kirtley, B. Kalisky, J. A. Bert, C. Bell, M. Kim, Y. Hikita, H. Y. Hwang, J. H. Ngai, Y. Segal, F. J. Walker, et al., Phys. Rev. B **85**, 224518 (2012).
[12] H. Padamsee, J. Knobloch, and T. Hays, *RF Superconductivities on Accelerators* (Wiley Series in Beam Physics and Accelerator Technology, 1998).
[13] C. P. Vlahacos, J. Matthews, and F. C. Wellstood, IEEE Trans. Appl. Supercond. **21**, 412 (2011).
[14] G. Ciovati, G. Myneni, F. Stevie, P. Maheshwari, and

D. Griffis, Phys. Rev. Special Topics-Accerlerators and Beams **13**, 022002 (2010).
[15] X. X. Xi, Supercond. Sci. Technol. **22**, 043001 (????).
[16] T. Tajima, A. Canabal, Y. Zhao, A. Romanenko, B. H. Moeckly, C. D. Nantista, S. Tantawi, L. Phillips, Y. Iwashita, and I. E. Campisi, IEEE Trans. Appl. Supercond. **17**, 1330 (2007).
[17] T. Tai, X. X. Xi, C. G. Zhuang, D. I. Mircea, and S. M. Anlage, IEEE Trans. Appl. Supercond. **21**, 2615 (2011).
[18] T. Tai, B. G. Ghamsari, T. Tan, C. G. Zhuang, X. X. Xi, and S. M. Anlage, Phys. Rev. ST Accel. Beams **15**, 122002 (2012).
[19] T. Tai, B. G. Ghamsari, and S. M. Anlage, IEEE Trans. Appl. Supercond. **23**, 7100104 (2013).
[20] T. Tai, B. G. Ghamsari, T. R. Bieler, T. Tan, X. X. Xi, and S. M. Anlage (2013), arXiv:1312.6257v1.
[21] R. O'Barr, M. Lederman, and S. Schultz, J. Appl. Phys. **79**, 6069 (1996).
[22] S. Y. Yamamoto and S. Schultz, Appl. Phys. Lett. **69**, 3263 (1996).
[23] S. Y. Yamamoto and S. Schultz, J. Appl. Phys. **81**, 4696 (1997).
[24] J. M. Pond, L. H. Allen, and E. J. Cukauskas, IEEE Trans. Appl. Supercond. **7**, 1857 (1997).
[25] F. H. Liu, S. Shi, J. Wang, Y. Chen, K. Stoev, L. Leal, R. Saha, H. Tong, S. Dey, and M. Nojaba, IEEE Trans. Appl. **37**, 613 (2001).
[26] M. R. Koblischka, J.-D. Wei, T. Sulzbach, A. D. Johnston, and U. Hartmann, IEEE Trans. on Magnetics **43**, 2205 (2007).
[27] M. R. Koblischka, J. D. Wei, and U. Hartmann, J. Magn. Magn. Mater. **322**, 1694 (2010).
[28] T. Tai, *Measuring electromagnetic properties of superconductors in high and localized RF magnetic field* (Ph.D dissertation; Univ. Maryland-College Park, http://hdl.handle.net/1903/14668, 2013).
[29] D. E. Oates, Y. D. Agassi, and B. H. Moeckly, IEEE Trans. Appl. Supercond. **17**, 2871 (2007).